Available online at www.sciencedirect.com
ScienceDirect
Journal of Power Sources 166 (2007) 400–410
JOURNAL OF POWER SOURCES
www.elsevier.com/locate/jpowsour

Nanoparticle gasifier fuel cell for sustainable energy future

Dimitri Gidaspow *, Veeraya Jiradilok

Illinois Institute of Technology, Chicago, IL, United States

Received 6 December 2006; received in revised form 20 December 2006; accepted 21 December 2006
Available online 17 January 2007

Abstract

A new concept for production of electricity from biomass or coal using molten carbonate fuel cells is proposed. It involves feeding fine coal particles or biomass, for sustainable energy future, with steam into the anode compartment of the fuel cell in which the waste heat from the fuel cell is used to produce synthesis gas which reacts electrochemically. This concept is illustrated using carbon nanoparticles as the fuel.

A computational fluid dynamics (CFD) model for the gasifier-fuel cell has been developed. Concentration, temperature and current density profiles have been computed. The computations show that practical current densities can be achieved. However, for the new concept to work well the carbon monoxide produced by the gasification should be allowed to react electrochemically. The computed temperature distributions for adiabatic operation show an initial drop in temperature due to gasification, followed by a rise which will have to be balanced by staggering the cells or by other means using the CFD design method.

Keywords: Molten carbonate fuel cell; Biomass gasification; Computational fluid dynamics; Nanotechnology; Carbon; Fluidization

1. Introduction

There is an urgent worldwide need to develop sustainable energy sources and means of production of nonpolluting electricity. Biomass is one such source of energy. It has been known for over a century than biomass particles, such as saw dust, can be used a source of fuel in a high temperature fuel cell to produce electricity. Unfortunately a direct feed of particles into a fuel cell gives very low current densities. Fig. 2.7-2 in Liebhafsky and Cairns's book [1] shows that fuel particles fed into a fuel cell do produce appreciable current. But for practical applications the current density must be increased by almost two orders of magnitude. This should be possible by feeding biomass or coal nanoparticles with steam into a high temperature fuel cell (Gidaspow's Patent application [2]).

2. Biomass gasification integrated with fuel cell literature

The use of carbon nanoparticles has recently been suggested [3–6] for the development of a direct carbon fuel cell, $C + O_2 \Leftrightarrow CO_2$, to take advantage of the fact that in an ideal situation all of the enthalpy of combustion of carbon can be transferred into electrical work in the reversible cell. In this innovative concept the carbon is dissolved in the molten carbonate electrolyte which is recirculated in the fuel cell and is oxidized at the anode. Although the concept proposed here is different, the idea of circulating the molten carbonate may be used to remove impurities, such as ash and sulfur found in coal. The solids produced will be removed using steam with a cyclic operation to clean the electrodes. The sulfur and ash will then removed by recirculating and filtering the electrolyte.

U.S. Patent 6,680,137 B2 [7] described a biomass gasification and fuel cell system. The fuel gas from the gasifier is directed to the anode of the fuel cell and at least a portion of the exhaust gas from the anode is directed to the combustor. The idea of gasification inside the fuel cell compartment is not described. This important new idea proposed here eliminates the expensive cryogenic air separation system in the Department of Energy FutureGen System for producing hydrogen from coal and using hydrogen in a fuel cell.

Donolo et al. [8] and Tomasi et al. [9] described the use of biomass in molten carbonate fuel cells. The gases are produced in separate gasifiers and reformers. Panopoulos et al. [10,11] described the use of a heat pipe to transfer heat from the fuel cell to the gasifier. Morita et al. [12] described electrochemical

* Corresponding author. Tel.: +1 312 567 3045; fax: +1 312 567 8874.
E-mail address: gidaspow@iit.edu (D. Gidaspow).

0378-7753/$ – see front matter © 2007 Elsevier B.V. All rights reserved.
doi:10.1016/j.jpowsour.2006.12.100

Nomenclature

C_d	drag coefficient
C_k	heat capacity of phase "k" (J kg^{-1} K^{-1})
C_p	heat capacity of gas (J kg^{-1} K^{-1})
C_C^0	initial concentration of fixed carbon in the particles
d_p	particle diameter (m)
D_i	bulk gas diffusivity of gas species i (m^2 s^{-1})
$D_{e,i}$	effective diffusivity of gas species i in the core (m^2 s^{-1})
$D_{M,i}$	effective diffusivity of gas species i in the shell (m^2 s^{-1})
$E(P_i)$	reversible emf of fuel cell (V)
E_0	Standard emf of fuel cell (V)
F	Faraday constant (C kmol^{-1})
g	gravitational acceleration (m s^{-2})
g_0	radial distribution function
G_s	solid modulus (Pa)
h	heat transfer coefficient (kg s^{-3} K^{-1} m^{-1})
h_{vk}	heat transfer coefficient (kg s^{-3} K^{-1})
H	enthalpy (J kg^{-1})
I	current density (A m^{-2})
K_g	gas phase heat transfer (kg m s^{-3} K^{-1})
$K_{p,i}$	mass transfer coefficient of gas species i through gas film surrounding a particle
K_r	rate constant (kmol (kmol C)$^{-1}$ atm^{-1} s^{-1})
K_s	particulate phase heat transfer (kg m s^{-3} K^{-1})
m_i^*	mass production or consumption (kg m^{-3} s^{-1})
M_i	molecular weight of species i (kg k mol^{-1})
n	number of electrons
Nu	Nusselt number
P	continuous phase pressure (atm)
Pr	Prandtl number
P_i	partial pressure (atm)
P_s	particulate phase pressure (atm)
P^*	equilibrium pressure (atm)
R	gas constant (8.314 kJ kmol^{-1} K^{-1})
Re	Reynolds number
R_{eff}	effective cell resistance of a molten carbonate fuel cell (ohm m^2)
R_i	rate of reaction of reaction i (kmol m^{-3} s^{-1})
t	time (s)
T	temperature (°C)
V	velocity (m s^{-1})
V_m	terminal cell potential (V)
W_C	weight fraction of carbon
Y_i	weight fraction of species i
X_i	mole fraction of species i

Greek letters

α	anode channel thickness
β	interphase transfer coefficient
γ_i	stoichiometric coefficient of reaction i
ε	volume fraction of phase "k"
η_i	effectiveness factor for the reaction in core
θ_C	void fraction of the particles in core
θ_S	void fraction of the particles in shell
μ	viscosity
ρ	density
ρ_{UC}	fraction radius of the unreacted core
ϕ_i	Thiele modulus for reaction i

Subscripts

s	solid phase
g	gas phase

production of current in a molten carbonate fuel cell with oxidation of hydrogen and carbon monoxide produced from biomass. At IIT Chuck [13] using a molten carbonate cell manufactured at IGT (Institute of Gas Technology), now GTI (Gas Technology Institute), systematically measured the current density of oxidation of carbon monoxide as a function of polarization from 10 to 70% inlet carbon monoxide concentration and temperatures of 750–875 °C. All the data were correlated by the relation current density equals Nernst potential minus voltage divided by cell resistance. The same model is used here.

3. Inherent efficiency of molten carbonate fuel cell systems for electricity production

Production of electricity from coal, biomass or organic waste according to the second law thermodynamics is best done using a fuel cell. In a fuel cell the differences of chemical potential of the fuel and air are forced to produce electric work [1]. In combustion the fuel and air are mixed producing heat, a random form of energy. Then this randomness is used to produce work using various cycles. Hence, inherently such systems are less efficient than those utilizing fuel cells. This is the advantage of gasification of fuels over combustion, as in the FutureGen project [14]. Unfortunately the present version of FutureGen involves gasification with oxygen to enable sequestration of carbon dioxide.

The new concept proposed here eliminates the oxygen plant and uses the waste heat from the fuel cell to supply the energy for production of synthesis gas in the same unit eliminating entropic losses due to heating and cooling. The molten carbonate fuel cells require carbon dioxide in the cathode for the transfer of carbonate ions [1]. Hence, they are the natural fuel cells to be used with fuels containing carbon, such as natural gas, coal or biomass. When the carbon dioxide is mixed with air in the cathode compartment at high concentrations, it provides additional electricity due to the differences in concentrations in the anode and the cathode. The carbon dioxide can be transferred from the anode to the cathode using a mass-exchanger in which the carbon dioxide reacts with potassium carbonate contained in a porous Teflon sheet [15]. The carbon dioxide is produced by the thermal decomposition of the product, bicarbonate using waste heat. Furthermore the carbon monoxide that will be present during the reaction with any carbonaceous fuel is itself electrochemically oxidized, and does not act as a poison [13].

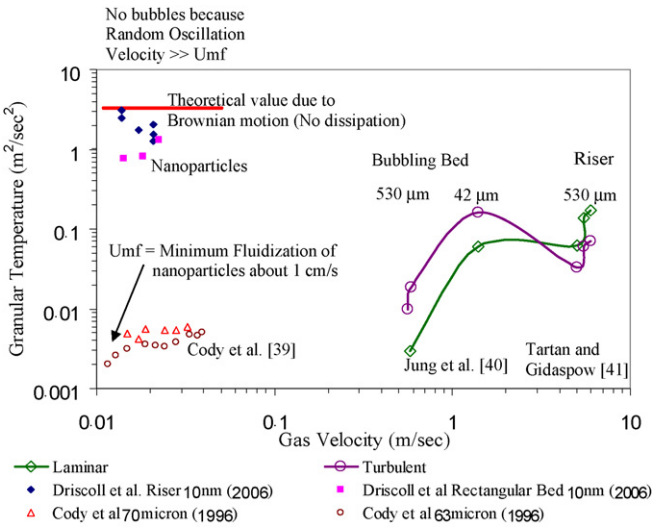

Fig. 1. The large random kinetic energy, Granular temperature, of nanoparticles [18] compared to micron size particles [39–41].

4. New concept

The new concept is based on our recent discovery of the unique flow properties of nanoparticles [16–18]. Nanoparticles fluidize without formation of bubbles due to their Brownian type interaction with air. Fig. 1 shows that their random kinetic energy, called granular temperature, is very high at rather low gas velocities. This random motion, of the order of 1 $m^2\,s^{-2}$ produces a mass flux equivalent to a current of 7 A cm^{-2}. Hence, mass transport of particles will not limit the performance of the fuel cell. The rate of gasification of the nanoparticles will also be very high due their small size.

Hence, the proposal is to feed carbon or biomass particles with steam into a molten carbonate fuel cell operating at about 600–800 °C, as shown in Fig. 2. In the fuel compartment of the fuel cell water will be split using biomass or carbon nanoparticles, with the additional energy supplied by the heat generated by the fuel cell. The hydrogen generated will react electrochemically to produce current. Unreacted fuel will be burned to maintain the high temperature and to provide the carbon dioxide to the cathode of the molten carbonate fuel cell.

The fuel cell will be initially similar to the molten carbonate fuel cell being commercialized by the Fuel Cell Energy Corporation, founded by the late Baker [19]. In these fuel cells, natural gas, essentially methane is internally reformed with steam to produce hydrogen which then reacts at current densities of over 100 mA cm^{-2} and an efficiency of about 50%. The concept has been scaled up to 1.8 MW [20] and is near commercialization. The novel idea proposed here is to use a storable fuel, carbon or biomass nanoparticles. Such a fuel cell battery can be used to power an automobile or a tractor without the need of an additional fuel. Nanoparticles will be stored in the fuel tank and delivered to the fuel cell with steam or carbon dioxide.

Commercial carbon nanoparticles are available. Biomass fuel, such as switch grass, has a high reactivity for reaction with steam [21].

5. Computational fluid dynamics (CFD) model

5.1. Hydrodynamics model

The CFD model is a predictive hydrodynamics multi-phase model developed to model fluidization [22,23] and nanoparticle flow [17]. In view of the measured nanoparticle viscosity and stresses we used the viscous model in Jiradilok et al. [17] to predict the hydrodynamics of nanoparticles in a gasifier fuel cell. The equations are the conservation of mass, momentum and energy equations for each phase given in Gidaspow's book as model B. All equations are written in rectangular coordinates, as summarized in Table 1 . These are $4(N+1)$ nonlinear-coupled partial differential equations for $4(N+1)$ dependent variables, for 1 gas phase and N solids phases. The variables to be computed

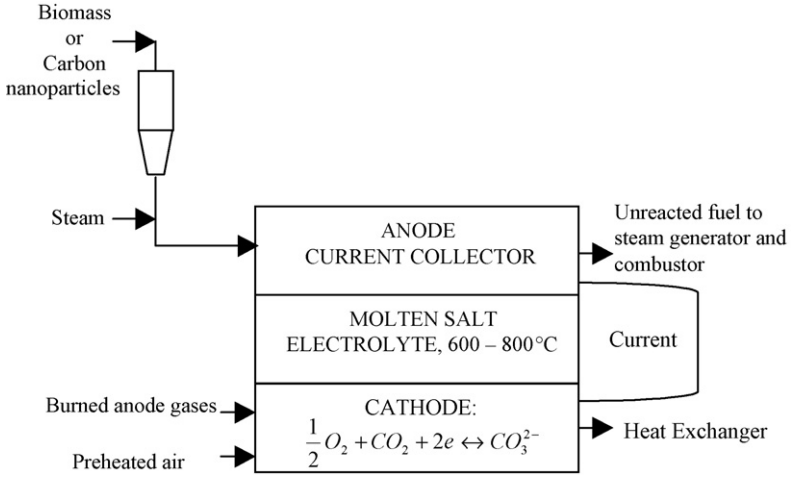

Fig. 2. Nanoparticle gasifier fuel cell. Anode reactions [34,33], gasification (for carbon feed), carbon steam reaction: $C + H_2O \rightarrow CO + H_2$ (endothermic $\Delta H = 32$ kcal $gmol^{-1}$); water shift reaction: $CO + H_2O \leftrightarrow CO_2 + H_2$ (exothermic $\Delta H = -9.8$ kcal $gmol^{-1}$); electrochemical reaction: $H_2 + CO_3^{2-} \rightarrow H_2O + CO_2 + 2e$ (exothermic $-\Delta H = (E - V)I - (T\,\Delta S/nF)I$.

Table 1
Mathematical model

Continuity equations

$$\frac{\partial}{\partial t}(\rho_i \varepsilon_i) + \nabla \cdot (\rho_i \varepsilon_i v_i) = \dot{m}_i \quad (i = \text{gas or solid})$$

Momentum equations

$$\frac{\partial(\rho_g \varepsilon_g v_g)}{\partial t} + \nabla \cdot (\rho_g \varepsilon_g v_g v_g) =$$
$$-\nabla P \bar{\bar{I}} + \nabla \cdot \bar{\bar{\tau}}_g - \beta_B (v_g - v_s) + \rho_g g$$
$$\frac{\partial(\rho_s \varepsilon_s v_s)}{\partial t} + \nabla \cdot (\rho_s \varepsilon_s v_s v_s) =$$
$$-\nabla P_s \bar{\bar{I}} + \nabla \cdot \bar{\bar{\tau}}_s + \beta_B (v_g - v_s) + \frac{\varepsilon_s}{\varepsilon_g}\left(\rho_s - \sum_{k=g,s}^{N} \varepsilon_k \rho_g\right) g$$

Energy equations

$$\frac{\partial}{\partial t}(\varepsilon_g \rho_g H_g) + \nabla \cdot (\varepsilon_g \rho_g H_g v_g) = \left(\frac{\partial P}{\partial t} + v_g \cdot \nabla P\right) + \sum_{k=1}^{N} h(T_k -$$
$$T_g) + \nabla \cdot (K_g \varepsilon_g \nabla T_g) + \varepsilon \sum_i R_{ig}\, \Delta H_{ig} + \varepsilon \sum_i^{H_2,CO} \Delta H_{i\,\text{fuel cell}}$$
$$\frac{\partial}{\partial t}(\varepsilon_s \rho_s H_s) + \nabla \cdot (\varepsilon_s \rho_s H_s v_s) = h(T_g - T_s) + \nabla \cdot (K_s \varepsilon_s \nabla T_s)$$

Constitutive equations

(1) Definitions: $\varepsilon_g + \varepsilon_s = 1$

(2) Gas pressure: $P_g = \rho_g \tilde{R} T_g$

(3) Stress tensor (i = gas or solid)

$$\bar{\bar{\tau}}_i = 2\mu_i \bar{\bar{D}}_i + (\lambda_i - \frac{2}{3}\mu_i)\,\text{tr}(\bar{\bar{D}}_i)\bar{\bar{I}} \text{ with } \bar{\bar{D}}_i = \frac{1}{2}[\nabla v_i + (\nabla v_i)^T]$$

(4) Empirical particulate phase viscosity and stress model

$$\nabla P_s = G(\varepsilon_g)\nabla \varepsilon_s \text{ with } G(\varepsilon_g) = 10^{-14.926\varepsilon_g + 18.667}\ \text{dyn cm}^{-2}$$
$$\mu_s = 0.017 \varepsilon_s^{1/3} g_0 \text{ (Poise)}$$

(5) Fluid-particulate interphase drag coefficients

for $\varepsilon < 0.8$ (based on the Ergun equation)

$$\beta = 150 \frac{\varepsilon_s^2 \mu_g}{\varepsilon_g^2 d_p^2} + 1.75 \frac{\rho_g \varepsilon_s}{\varepsilon_g d_p} |v_g - v_s|$$

for $\varepsilon \geq 0.8$ (based on the empirical correlation)

$$\beta = \frac{3}{4} C_d \frac{\rho_g \varepsilon_s |v_g - v_s|}{d_p} \varepsilon_g^{-2.65}$$

where $C_d = \dfrac{24}{Re_p}[1 + 0.15 Re_p^{0.697}]$ for $Re_p < 1000$ and $C_d = 0.44$ for $Re_p > 1000$

(6) Enthalpy

$$H_g = C_{p_g}(T_g - T_g^0)$$
$$H_s = C_{p_s}(T_s - T_s^0)$$

where T_g^0, T_s^0: the standard temperature, 25 °C, 298 K

(7) Heat transfer coefficients

(7.1) Gas-particle heat transfer coefficient, h_{vk}

for $\varepsilon \leq 0.8$

$$Nu_k = (2 + 1.1 Re^{0.6} Pr^{1/3}) S_k \ (Re \leq 200)$$
$$= 0.123 \left(\frac{4Re}{d_k}\right)^{0.83} S_k^{0.17} \ (200 \leq Re \leq 2000)$$
$$= 0.61 Re^{0.67} S_k \ (Re > 2000)$$

for $\varepsilon > 0.8$

$$Nu_k = (2 + 0.16 Re^{0.67}) S_k \ (Re \leq 200)$$
$$= 8.2 Re^{0.6} S_k \ (200 \leq Re \leq 1000)$$
$$= 1.06 Re^{0.457} S_k \ (Re > 1000)$$

where $Re = \frac{\varepsilon_g \rho_g |\bar{v}_g - \bar{v}_k| d_k}{\mu_g}$, $Pr = \frac{c_{p,g}\mu_g}{K_g}$, $S_k = \varepsilon_k \frac{6}{d_k}$,
$Nu = \frac{h_{vk} d_k}{K_g^0}$, $h = \frac{6\varepsilon_s}{d_p} h_{vk}$ [36]

Table 1 (*Continued*)

(7.2) Gas heat transfer coefficient

$$K_g^0 = 8.64 \times 10^5 \left(\frac{T_g}{1400}\right)^{1.786} (\text{g cm s}^{-3}\text{K}^{-1})$$
$$K_g = (1 - \sqrt{\varepsilon_s}) K_g^0$$

(7.3) Particle heat transfer coefficient, K_k [23]

$$\frac{K_k}{K_g^0} = (1 - \sqrt{\varepsilon_s}) + \sqrt{\varepsilon_s}\left[\varphi R + (1 - \varphi)\frac{\lambda_{so}^*}{\lambda}\right]$$

with $\dfrac{\lambda_{so}^*}{\lambda} =$

$$\frac{2}{1 - B/R}\left(\frac{B/R(R-1)}{(1 - B/R)^2} \times \ln\frac{B}{R} - \frac{B-1}{1 - B/R} - \frac{B+1}{2}\right), \quad R = \frac{K_p}{K_g^0}, \quad B = 1.25\left(\frac{1 - \varepsilon_g}{\varepsilon_g}\right)^{10/9}, \quad \varphi = 7.26 \times 10^{-3}$$

are the pressure P, the solids volume fractions ε_k ($k = 1, \ldots, N$), the gas velocity components U_g and V_g and the solids velocity components U_k and V_k ($k = 1, \ldots, N$) in the $-x$ and $-y$ direction, respectively, and the temperature T_g and T_k ($k = 1, \ldots, N$) of gas and solids phases, respectively. The numerical scheme used in the IIT code is the Implicit Continuous Eulerian (ICE) approach. The model uses donor cell differencing. The conservation of momentum and energy equations are in mixed implicit form. The continuity equations excluding mass generation are in implicit form. In this study there is one solids phase.

The solid viscosity and solids modulus are input data into the viscous model. The solid viscosity increases with increasing solid concentration, which was estimated as a function of radial distribution function [17]:

$$\mu_s = 0.0017 \varepsilon_s^{1/3} g_0 \quad (\text{Pa s}) \tag{1}$$

The above expression for the solids viscosity is based on the experimental data. The radial distribution function at contact, g_0, is calculated as follows:

$$g_0 = \left[1 - \left(\frac{\varepsilon_s}{\varepsilon_{s,\max}}\right)^{1/3}\right]^{-1} \tag{2}$$

where the maximum solids packing, $\varepsilon_{s,\max}$ was estimated from the solid compression in the IIT fluidized bed and simulation data which was 0.08.

The correlation for particulate viscosity given by Eq. (1) is a semi-empirical equation based on kinetic theory. The viscosity increases to the one-third power due to isentropic compression [24]. The radial distribution function is based on Bagnold's equation. It is similar to the viscosity of a concentrated suspension of Frankel and Acrivos [25].

The solid stress modulus of nano-size particle for 10 nm Tullanox was estimated by Jung and Gidaspow [26]. They measured the solid volume fraction as a function of bed height using a γ-ray densitometer in a settling experiment giving the solid pressure as a function of the solids volume fraction. Hence, the derivative of solid pressure equals the solid stress modulus. The solid modulus is expressed as a function of the gas volume fraction. An exponential form is used.

$$G(\varepsilon_g) = 10^{-14.926\varepsilon_g + 18.667} \quad (\text{dyn cm}^{-2}) \tag{3}$$

The gas and solids phase energy equations are written in their enthalpy form. The viscous dissipation of two phases and the slip work between phases were assumed to be not important and were not included in the energy equation. There are two important heat sources, endothermic heat from gasification reactions and exothermic heat from fuel cell. Therefore, in the fuel compartment of the fuel cell water will be split using carbon nanoparticles, with the additional energy supplied by the heat generated by the fuel cell. The hydrogen and carbon monoxide generated will react electrochemically to produce current.

5.2. Gasification

5.2.1. Description of gasifier

The gasification reactions are similar to those for a moving-bed coal gasification reactor of Yoon et al. [27]. The dominant processes of the gasification are heterogeneous reactions between carbon and components of the gas phase.

The gasification reactions consist of three reactions as follows:

$$\text{Reaction 1}: \quad C + CO_2 \rightarrow 2CO$$

$$\text{Reaction 2}: \quad C + 2H_2 \rightarrow CH_4$$

$$\text{Reaction 3}: \quad C + H_2O \rightarrow CO + H_2$$

In addition to the three heterogeneous reactions, the water gas shift reaction occurs in the gas phase catalyzed by carbon particles.

$$\text{Water shift reaction}: \quad CO + H_2O \Leftrightarrow CO_2 + H_2$$

Skinner and Smoot [28] have reviewed the literature of the reactions of char and carbon.

5.2.2. Model

For the gasification the conservation of species equations are added into the code to describe gasification reactions. The left-hand side terms of the continuity equations for solids and gas phase do not equal to 0 due to mass changing with reactions. They are summarized as follows:

- Continuity equation for solid phase:

$$\frac{\partial}{\partial t}(\rho_s \varepsilon_s) + \nabla \cdot (\rho_s \varepsilon_s V_s) = M_C(-R_1 - R_2 - R_3) \tag{4}$$

- Continuity equation for gas phase:

$$\begin{aligned}\frac{\partial}{\partial t}(\rho_g \varepsilon_g) + \nabla \cdot (\rho_g \varepsilon_g V_g) &= R_1(-M_{CO_2} + 2M_{CO}) + R_2(-2M_{H_2} + M_{CH_4}) \\ &+ R_3(M_{CO} + M_{H_2} - M_{H_2O}) \\ &+ R_4(M_{CO_2} - M_{CO} + M_{H_2} + M_{H_2O})\end{aligned} \tag{5}$$

- The conservation of species balance in solid phase:

component balance for C :

$$\frac{\partial}{\partial t}(\rho_s \varepsilon_s W_C) + \nabla \cdot (\rho_s \varepsilon_s W_C V_s) = M_C(-R_1 - R_2 - R_3) \tag{6}$$

- The conservation of species balance in gas phase:

component balance for CO_2 :

$$\frac{\partial}{\partial t}(\rho_g \varepsilon_g Y_{CO_2}) + \nabla \cdot (\rho_g \varepsilon_g Y_{CO_2} V_g) = M_{CO_2}(-R_1 + R_4) \tag{7}$$

component balance for CO :

$$\frac{\partial}{\partial t}(\rho_g \varepsilon_g Y_{CO}) + \nabla \cdot (\rho_g \varepsilon_g Y_{CO} V_g) = M_{CO}(2R_1 + R_3 - R_4) \tag{8}$$

component balance for H_2 :

$$\frac{\partial}{\partial t}(\rho_g \varepsilon_g Y_{H_2}) + \nabla \cdot (\rho_g \varepsilon_g Y_{H_2} V_g) = M_{H_2}(-2R_2 + R_3 + R_4) \tag{9}$$

component balance for CH_4 :

$$\frac{\partial}{\partial t}(\rho_g \varepsilon_g Y_{CH_4}) + \nabla \cdot (\rho_g \varepsilon_g Y_{CH_4} V_g) = M_{CH_4} R_2 \tag{10}$$

component balance for H_2O :

$$\frac{\partial}{\partial t}(\rho_g \varepsilon_g Y_{H_2O}) + \nabla \cdot (\rho_g \varepsilon_g Y_{H_2O} V_g) = M_{H_2O}(-R_3 + R_4) \tag{11}$$

where Y_i is the weight fraction of species i in gas phase and W_C is the weight fraction of carbon.

5.2.3. Kinetic study

5.2.3.1. Heterogeneous reaction model. The shrinking core model used to calculate the rate of the heterogeneous reaction is given by:

$$R_i = \frac{\varepsilon_s(P_i - P_i^*)}{(d_p/6K_{p,i}) + (d_p^2(1-\rho_{UC})RT/12\rho_{UC}D_{M,i}) + (1/\eta_i \rho_{UC}^3 K_{r,i} C_C^0)} \tag{12}$$

Similar to that given by Yoon et al. [27] there are three main resistances in this model, mass transfer, diffusion and reaction effects. In the system of flow of nanoparticles, the first two effects, mass transfer and diffusion are small due to the small particle diameter. The reaction part in the shrinking core model plays the important role.

The effectiveness factor for the reaction in the core, η_i, is defined by:

$$\eta_i = \frac{1}{\phi_i}\left(\frac{1}{\tanh(3\phi_i)} - \frac{1}{3\phi_i}\right) \tag{13}$$

The Thiele modulus for reaction i is defined by:

$$\phi_i = \frac{d_p \rho_{UC}}{6}\sqrt{\frac{K_{r,i} C_C^0}{\gamma_i D_{e,i}/RT}} \tag{14}$$

The effective diffusivities in the outer shell and also in the core of the particles are estimated by Walker et al. [29] as follows:

$$\text{Shell}: \quad D_{\mathrm{M},i} = D_i \theta_{\mathrm{S}}^2 \tag{15}$$

$$\text{Core}: \quad D_{\mathrm{e},i} = D_i \theta_{\mathrm{C}}^2 \tag{16}$$

The Gasification reactions consist of three heterogeneous reactions as follows:

$$\text{Reaction 1}: \quad \mathrm{C} + \mathrm{CO_2} \rightarrow 2\mathrm{CO}$$

$$(\Delta H^0_{\mathrm{R},1}|_{298\,\mathrm{K}} = 40.273\,\mathrm{kcal\,gmol^{-1}}) \tag{17}$$

$$K_{\mathrm{r,CO_2}} = 930 \exp\left(-\frac{45,000}{RT_{\mathrm{S}}}\right)$$

$$(\mathrm{gmol\,(gmol\,C)^{-1}\,atm^{-1}\,s^{-1}}) \tag{18}$$

$$K_{\mathrm{eq}} = \frac{P^2_{\mathrm{CO}}}{P^*_{\mathrm{CO_2}}} = 1.222 \times 10^9 \exp\left(-\frac{40,300}{RT_{\mathrm{S}}}\right) \tag{19}$$

$$P^*_{\mathrm{CO_2}} = \frac{P^2_{\mathrm{CO}}}{1.222 \times 10^9 \exp\left(-40,300/RT_{\mathrm{S}}\right)} \tag{20}$$

The rate constant, $K_{\mathrm{r,CO_2}}$, is for Pittsburgh 8 coal [30]. Skinner and Smoot [28], Table 2 gives the Arrhenius constants for reaction 1 for charcoal, coke etc. The equilibrium constant, K_{eq}, is the one given in Yoon et al. [27].

$$\text{Reaction 2}: \quad \mathrm{C} + 2\mathrm{H_2} \rightarrow \mathrm{CH_4}$$

$$(\Delta H^0_{\mathrm{R},2}|_{298\,\mathrm{K}} = -21.849\,\mathrm{kcal\,gmol^{-1}}) \tag{21}$$

$$K_{\mathrm{r,H_2}} = 8.36 \times 10^{-4} \exp\left(-\frac{1650}{RT_{\mathrm{S}}}\right)$$

$$(\mathrm{gmol\,(gmol\,C)^{-1}\,atm^{-1}\,s^{-1}}) \tag{22}$$

Table 2
System geometry, all properties the gas and the solid and operating conditions

Fluidized bed dimension	
Height	30.00 cm
Width	10.85 cm
Number of cell × cell size in x direction	31 × 0.35 cm
Number of cell × cell size in y direction	20 × 1.5 cm
Fluid properties	
Initially the bed was filled with the N_2	
Steam, H_2O was fed into the bed.	
Solid properties	
Initially the bed was filled with the carbon nanoparticles	
Agglomerate particle diameter	204 μm
Agglomerate particle density	440 kg m^{-3}
Initial solid volume fraction for agglomerate particles	0.44
Operating conditions	
Pressure	1 atm
Temperatures	750 °C
Inlet velocity of steam, H_2O	3.20 cm s^{-1}
Initial bed height	4.50 cm
Initial weight fraction of C particles	0.95
Time interval, Δt	10^{-5} s

$$K_{\mathrm{eq}} = \frac{P_{\mathrm{CH_4}}}{(P^*_{\mathrm{H_2}})^2} = 1.5 \times 10^{-6} \exp\left(\frac{21848.52}{RT_{\mathrm{S}}}\right) \tag{23}$$

$$P^*_{\mathrm{H_2}} = \sqrt{\frac{P_{\mathrm{CH_4}}}{1.5 \times 10^{-6} \exp\left(21848.52/RT_{\mathrm{S}}\right)}} \tag{24}$$

The rate constant, $K_{\mathrm{r,H_2}}$, is given in Yoon et al. [27]. However, the activation energy used is much lower. Hence, there is essentially no methane production.

$$\text{Reaction 3}: \quad \mathrm{C} + \mathrm{H_2O} \rightarrow \mathrm{CO} + \mathrm{H_2}$$

$$(\Delta H^0_{\mathrm{R},3}|_{298\,\mathrm{K}} = 32.432\,\mathrm{kcal\,gmol^{-1}}) \tag{25}$$

$$K_{\mathrm{r,CO_2}} = 930 \exp\left(-\frac{45,000}{RT_{\mathrm{S}}}\right)$$

$$(\mathrm{gmol\,(gmol\,C)^{-1}\,atm^{-1}\,s^{-1}}) \tag{26}$$

$$K_{\mathrm{eq}} = \frac{P_{\mathrm{H_2}} P_{\mathrm{CO}}}{(P^*_{\mathrm{H_2O}})^2} = \exp\left(17.2931 - \frac{16326.1}{T_{\mathrm{S}}}\right) \tag{27}$$

$$P^*_{\mathrm{H_2O}} = \sqrt{\frac{P_{\mathrm{H_2}} P_{\mathrm{CO}}}{\exp\left(17.2931 - 16326.1/T_{\mathrm{S}}\right)}} \tag{28}$$

The numerical values are for Pittsburgh 8 coal. They are similar to those of Yoon et al. [27]. Skinner and Smoot [28] give the Arrhenius constants for graphite, charcoal and coke.

Water shift reaction [27]:

$$\mathrm{CO} + \mathrm{H_2O} \Leftrightarrow \mathrm{CO_2} + \mathrm{H_2}$$

$$(\Delta H^0_{\mathrm{R},4}|_{298\,\mathrm{K}} = -9.838\,\mathrm{kcal\,gmol^{-1}}) \tag{29}$$

$$R_4 = 0.775 \exp\left(\frac{-8421.3}{T_{\mathrm{G}}}\right) P^{0.5-P/250} \times \left(X_{\mathrm{CO}} X_{\mathrm{H_2O}} - \frac{X_{\mathrm{CO_2}} X_{\mathrm{H_2}}}{K_{\mathrm{wg}}}\right)(1 - W_{\mathrm{C}})\rho_{\mathrm{C}}\varepsilon_{\mathrm{S}}$$

$$(\mathrm{gmol\,cm^{-3}\,s^{-1}}) \tag{30}$$

$$K_{\mathrm{wg}} = 0.0265 \exp\left(\frac{7860}{RT_{\mathrm{G}}}\right) \tag{31}$$

Wen [31] reviewed the details of the shift reaction.

5.3. Gasifier fuel cell

5.3.1. Description of gasifier fuel cell

A complete derivation of the basic model equation $I_i = (E(P_i) - V_E)/R_{eff}$ to obtain the current density is given in Dharia [32], in Gidaspow's report [33,34] and his book [35].

The fuel cells produce electricity by the electrochemical oxidation of hydrogen and carbon monoxide. The half-cell reactions are:

- Hydrogen system:

Anode	$H_2 + CO_3^{-2} \leftrightarrow H_2O + CO_2 + 2e^-$
Cathode	$1/2O_2 + 2e^- + CO_2 \leftrightarrow CO_3^{2-}$
Overall	$H_2 + 1/2O_2 \leftrightarrow H_2O$

- Carbon monoxide system:

Anode	$CO + CO_3^{2-} \leftrightarrow 2CO_2 + 2e^-$
Cathode	$CO_2 + 1/2O_2 + 2e^- \leftrightarrow CO_3^{2-}$
Overall	$CO + 1/2O_2 \leftrightarrow CO_2$

5.3.2. Model

For the hydrogen-carbon monoxide gasifier fuel cell the conservation of species equations of hydrogen and carbon monoxide are added into the gasification code to describe electrochemical reactions. The left-hand side term of the continuity equation for gas phase does not equal to 0 due to mass changing with gasification and electrochemical reactions. They are summarized as follows:

- Continuity equation for gas phase:

$$\frac{\partial}{\partial t}(\rho_g \varepsilon_g) + \nabla \cdot (\rho_g \varepsilon_g V_g) = R_1(-M_{CO_2} + 2M_{CO}) + R_2(-2M_{H_2} + M_{CH_4}) + R_3(M_{CO} + M_{H_2} - M_{H_2O}) + R_4(M_{CO_2} - M_{CO} + M_{H_2} + M_{H_2O}) - \frac{I}{nF\alpha}M_{H_2} - \frac{I}{nF\alpha}M_{CO} \quad (32)$$

- The conservation of species balance in gas phase:

component balance for H_2 :

$$\frac{\partial}{\partial t}(\rho_g \varepsilon_g Y_{H_2}) + \nabla \cdot (\rho_g \varepsilon_g Y_{H_2} V_g) = M_{H_2}(-2R_2 + R_3 + R_4) - \frac{I}{nF\alpha}M_{H_2} \quad (33)$$

component balance for CO :

$$\frac{\partial}{\partial t}(\rho_g \varepsilon_g Y_{CO}) + \nabla \cdot (\rho_g \varepsilon_g Y_{CO} V_g) = M_{CO}(2R_1 + R_3 - R_4) - \frac{I}{nF\alpha}M_{CO} \quad (34)$$

The reversible emf of fuel cell, $E(P_{H_2})$ and $E(P_{CO})$ are obtained from the Nernst equation, calculated as a function of concentration of hydrogen and carbon monoxide as follows:

$$E(P_{H_2}) = E_0 + \frac{RT}{2F}\ln\frac{P_{H_2}P_{O_2}^{1/2}}{P_{H_2O}} \quad (V) \quad (35)$$

$$E(P_{CO}) = E_0 + \frac{RT}{2F}\ln\frac{P_{CO}P_{O_2}^{1/2}}{P_{CO_2}} \quad (V) \quad (36)$$

Rate consumption of hydrogen and carbon monoxide in a fuel cell is $I_i/n_i F\alpha$ (mol cm^{-3} s^{-1}), where I_i is the current density (A cm^{-2}), n_i: 2 (number of electron produced per H_2 mole); 2 (number of electron produced per CO mole), F: 96,500 C mol^{-1}, α: 2 mm, thickness of anode channel.

5.4. Initial condition and boundary condition

To solve the equations listed in Table 1, appropriate initial and boundary conditions are needed. The initial conditions can be specified according to the computed system. In this study, we simulated the gasifier fuel cells in a batch mode. At the inlet, the gas velocity, the gas compositions, gas temperature and pressure were prescribed. In the reactor, the carbon nanoparticles were contained at minimum fluidizing velocity. Therefore, the volume fractions, velocities, compositions, temperatures of gas and solids phases and pressure were prescribed. The simulations were carried out for a two-dimensional fluidized bed. The system geometry, all properties the gas and the solid and operating conditions are summarized in Table 2.

5.4.1. Initial conditions for gasifier fuel cell

In the simulations, only the anode is simulated. The concentration of oxygen, P_{O_2}, is assumed to be constant. The gases produced from the fuel cell, carbon dioxide and steam, P_{CO_2} and P_{H_2O}, are also assumed to be constant with no feedback to gasification. The mole fractions of oxygen, carbon dioxide and steam are 0.21, 0.01 and 0.01, respectively. The standard emf of a fuel cell is $E_0 = 1.2605 - 0.00025T$. The terminal cell potential, V_m, was varied to be 0.8 and 0.6 V. The effective cell resistance for a molten carbonate fuel cell, R_{eff}, estimated from the slope of cell potential and current density is 1.987 ohm cm^2 [32]. Chuck [13] had shown that the polarization of the carbon monoxide fuel cell at 875 °C is the same as that of the hydrogen fuel cell at 800 °C. Hence here we used the same resistance for the carbon monoxide fuel cell.

5.4.2. Boundary conditions

At an impenetrable solid wall the gas velocities in two directions are generally set to be zero. The no-slip condition was applied for solids phase. At the outlet, the mass flux is assumed to be continuous.

6. CFD simulations

During the energy crisis in 1970s, the design of gasifiers and fluidized bed combustors could not be done from first principles due to a lack of understanding of gas-particle flow. With funding from National Science Foundation and Department of Energy

in 1980s and 1990s and the development of fast computers it became possible to solve the coupled Navier–Stokes equations using the computational fluid dynamics (CFD) approach.

An example of the acceptance of CFD in the fluidization community is the plenary lecture by Kuippers et al. [36] at Fluidization IX. Two plenary lectures in the Flour–Daniel AIChE lecture series have summarized the progress made in the last decade. Jackson's [37] 1994 lecture discussed the equations of motion and hydrodynamic instability, while Arastoopour's [38] 1999 lecture emphasized their numerical solution. Commercial codes, such as *Fluent*, allow the solution of transient multi dimensional problems. Gidaspow [35] had reviewed the theory.

Table 1 summarizes the conservations of mass, momentum and energy equations for the gases and the particles. The conservations of species equations are shown in the gasification and gasifier fuel cell sections. The gasification reactions are similar to those for a moving-bed coal gasification reactor of Yoon et al. [27]. The molten carbonate fuel cell model is based on the research at The Institute of Gas Technology and Fuel Cell Energy Corporation as reviewed by Gidaspow [34]. In the present simulations the gasification kinetics were limited by the rates of chemical reactions determined for large coal particles. For nanoparticles we expect the rates of reactions to be much higher due to their large surface area.

Figs. 3–7 show our simulations for a fuel cell reactor at isothermal conditions, 30.0 cm × 10.9 cm, initially filled with close to pure carbon up to the height of 4.5 cm fluidized with nitrogen. Fig. 3a shows the carbon distribution after 20 s of reactions. Fig. 3b and c shows the hydrogen concentration and the current density, respectively. In this simulation the inlet steam velocity was low, 3.2 cm s^{-1} and the bed was only partially filled

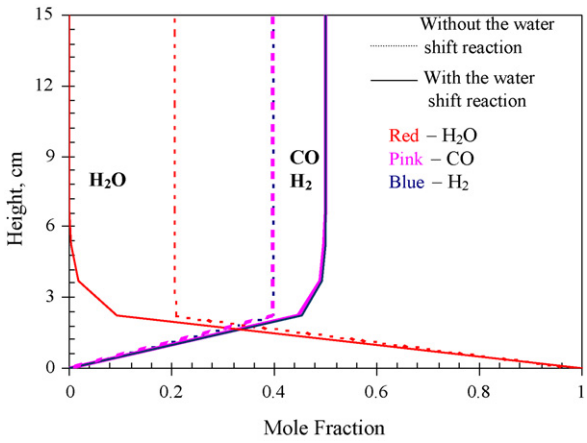

Fig. 4. Gasification axial profiles with no current production, 1023 K, 3.2 m s^{-1} steam.

with carbon. Hence, the reaction and current generation were all at the bottom of the reactor. The current density in Fig. 3c is with no carbon monoxide reaction. In a later section, it is shown that the current density is higher when carbon monoxide reacted electrochemically.

Fig. 4 shows gasification with and without the shift reaction. With the water shift reaction the hydrogen concentration increases from 40 to 50%. Similar to the Lurgi gasifier [27] there is appreciable carbon monoxide formation.

Fig. 5 shows the compositions in the gasifier fuel cell fed with a low steam velocity, 3.2 cm s^{-1} and a high steam velocity, 32 cm s^{-1}. At the low velocity no hydrogen leaves the reactor. The product is almost all carbon monoxide. At the high velocity, about 40% hydrogen and 50% carbon monoxide leave the

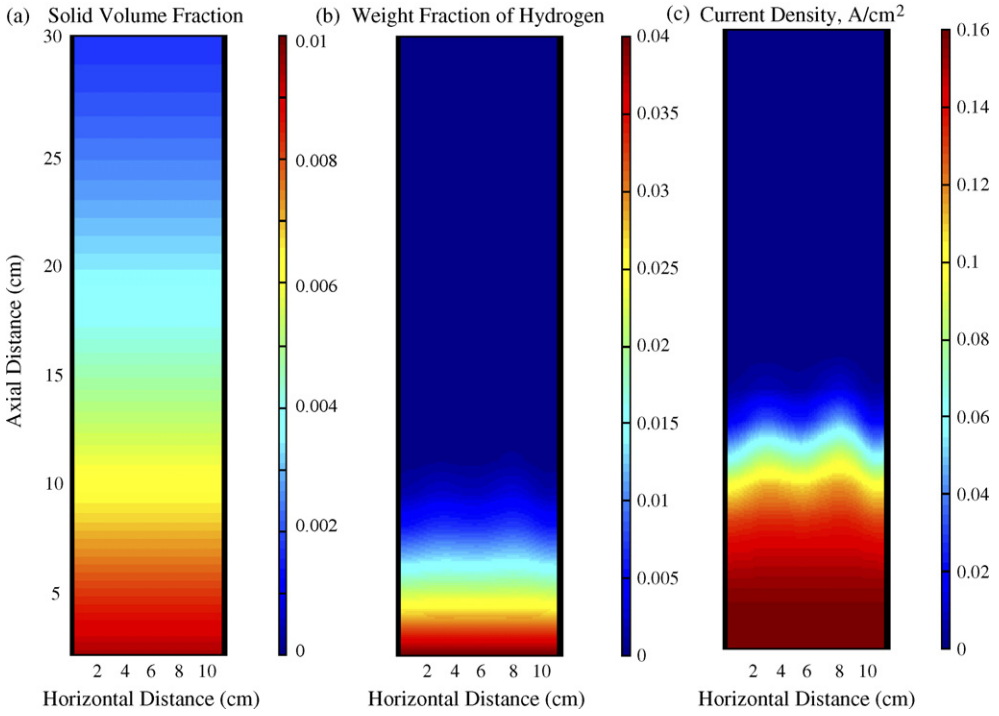

Fig. 3. Computed (a) solid volume fraction of carbon, (b) weight fraction of hydrogen and (c) current density at 0.8 V with no electrochemical reaction of carbon monoxide, 1023 K.

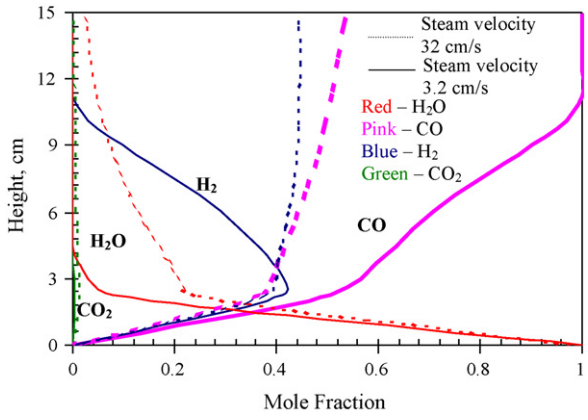

Fig. 5. Concentration axial profiles of a gasifier fuel cell, with no electrochemical reaction of carbon monoxide, at high and low steam velocities, 1023 K, 0.8 V.

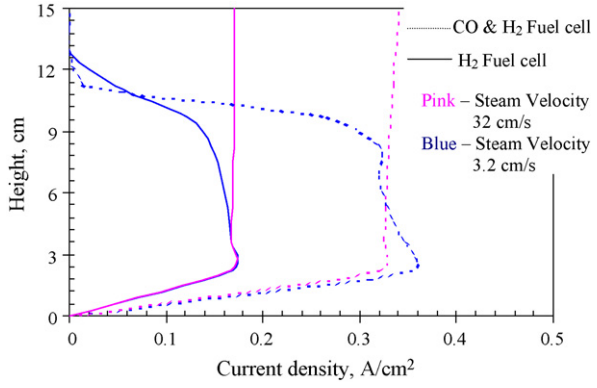

Fig. 6. Current density axial profiles of gasifier hydrogen and carbon monoxide fuel cells, operating at high and low steam velocities, 1023 K, 0.8 V.

cell. In the first study, we assumed that carbon monoxide does not contribute to the formation of current. In the molten carbonate fuel cell it was shown by Chuck [13] that carbon monoxide can be oxidized electrochemically to produce reasonable current densities. Morita et al. [12] computed the electrochemical work output from the molten carbonate fuel cell by considering both the electrochemical oxidization of hydrogen and carbon

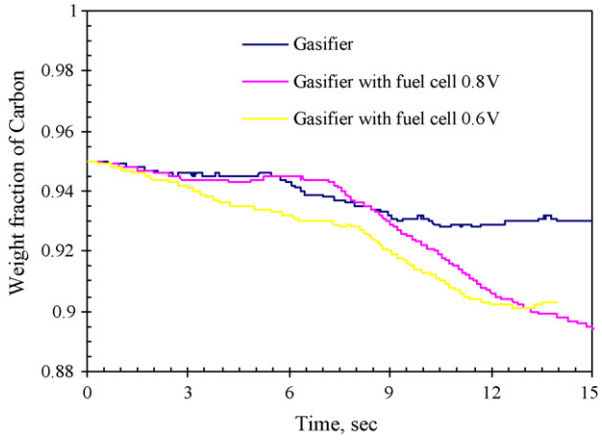

Fig. 7. Carbon conversion in a batch mode as a function of operating time, at 1023 K, 3.2 cm s^{-1} steam.

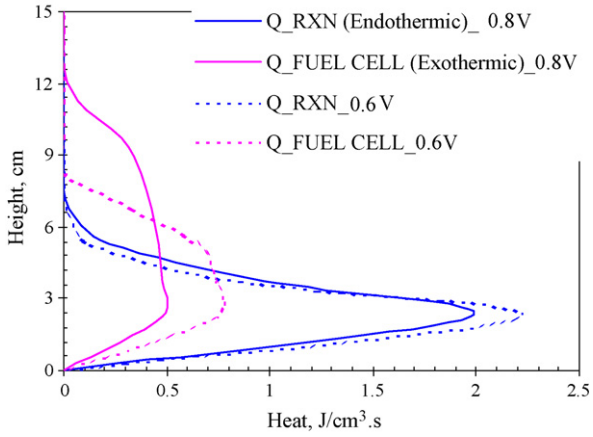

Fig. 8. Heat generation in the fuel cell with hydrogen oxidation only and gasification at 0.8 and 0.6 V, 3.2 m s^{-1}.

monoxide. Hence, in the next modeling study we included the production of current due to the electrochemical oxidation of carbon monoxide.

Fig. 6 shows the current densities for the low and high steam velocities with an electrochemical production of current by hydrogen and carbon monxide. At the high steam velocity the current density is uniform, except at the inlet. The current density with electrochemical carbon monoxide reaction is double that with hydrogen oxidation only.

Fig. 7 shows the weight fraction of carbon conversion as a function of operating time in the gasifier only and the gasifier fuel cell operating at 0.8 and 0.6 V. Gasification speeds up with a fuel cell due to the shift in equilibrium. We plan to simulate the gasifier fuel cells in a batch and continuous carbon feed modes and find optimum operating conditions.

Figs. 8–11 show the operation of gasifier fuel cells at adiabatic conditions. The initial temperature was 1023 K. Figs. 8 and 9 show that we have to supply heat at the inlet of the gasifier fuel cell and remove it in the second part of the reactor. The corresponding temperature profiles in Fig. 10 shows a drop in the temperature near the inlet followed by a rise. The drop in temperature in the upper portion of the system is due to the transient operation at the low steam velocity. There is no reaction in

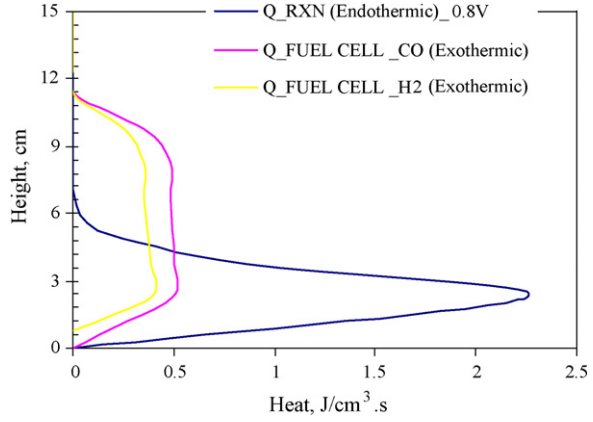

Fig. 9. Heat generation in the hydrogen–carbon monoxide gasifier fuel cell at 0.8 V, 3.2 m s^{-1}.

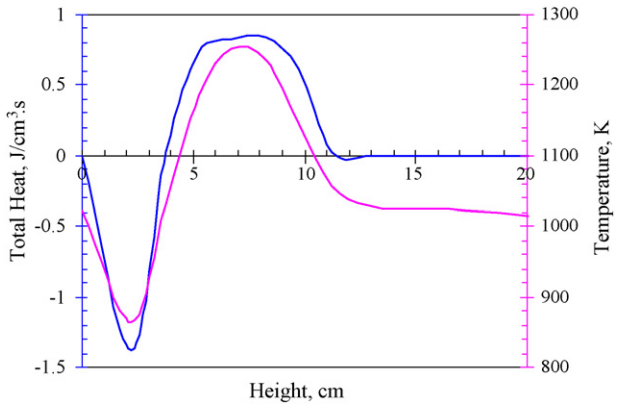

Fig. 10. Temperature and total heat profiles of hydrogen–carbon monoxide gasifier fuel cell at 0.8 V, 3.2 m s^{-1}.

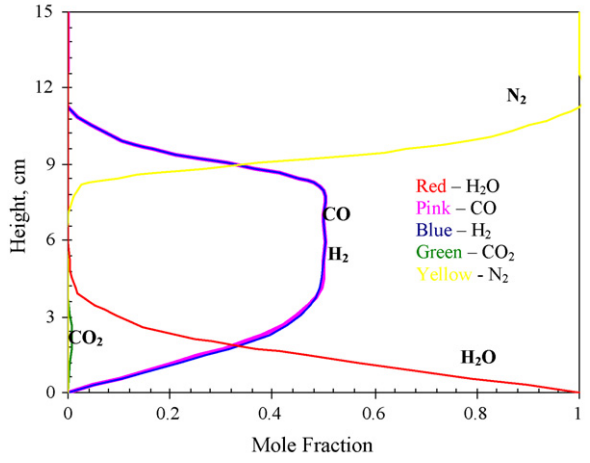

Fig. 11. Concentration axial profiles of a hydrogen–carbon monoxide gasifier fuel cell, at 0.8 V, 3.2 m s^{-1} at adiabatic conditions.

the top part. An optimum steam velocity needs to be determined. We also plan to add the cathode stream and the boiler to produce steam.

Fig. 11 shows the concentration profiles at adiabatic conditions for the gasifier carbon monoxide–hydrogen fuel cell. The computed temperature distributions for adiabatic operation show an initial drop in temperature due to gasification, followed by a rise which will have to be balanced by staggering the cells or by other means using the CFD design method. Unlike at isothermal conditions shown in Fig. 5, here the carbon monoxide decreased to zero at the outlet. Hence, here we have a complete conversion of hydrogen and carbon monoxide.

7. Conclusions

(1) Traditionally [31] coal gasification processes were optimized using measured rates of gasification reactions and macroscopic type balances of species and energy, such as now found in commercial codes like ASPEN. The development of multiphase flow theory [35] and fast computers now permits the detailed design of such reactors using computational fluid dynamics. This study provides an example of such an approach using a nanoparticle size CFD model of Jiradilok et al. [17].

(2) Integration of gasification and molten carbonate fuel cells has been previously suggested in the literature. Here, we show using CFD calculations that gasification and electricity production can be done in the same unit, similarly to the production of electricity from natural gas with internal reforming using the molten carbonate fuel cell.

(3) Fig. 11 shows that carbon monoxide will react completely in the fuel cell with electrochemical reaction. With no reaction, Fig. 5 shows that it will leave the fuel cell gasifier partially unreacted. Hence, to take full advantage of the new concept, carbon monoxide will have to react electrochemically in the fuel cell gasifier.

Acknowledgment

This study was supported by the U.S. Department of Energy grant (DE-FG26-06NT42736).

References

[1] H.A. Liebhafsky, E.J. Cairns, Fuel Cells and Fuel Batteries, 1st ed., Wiley, New York, 1968 (based on Fig. 2.7-2, pp. 37).
[2] D. Gidaspow, Nanoparticle Gasifier Fuel Cell: Patent Application, Illinois Institute of Technology, 2006.
[3] J.F. Cooper, N. Cherepy, R. Upadhye, A. Pasternak, M. Steinberg, Direct Carbon Conversion: Review of Production and Electrochemical Conversion of Reactive Carbons, Economics and Potential Impact on the Carbon Cycle, Report Number: UCRL-ID-141818, 2000.
[4] J.F. Cooper, Reactions of the Carbon Anode in Molten Carbonate Electrolyte, 2003 Conference Proceedings Direct Carbon Fuel Cell Workshop, Lawrence Livermore National Laboratory, 2003.
[5] K. Hemmes, in: R.E. White, Vayenas (Eds.), Fuel Cells, Chapter in Modern Aspects of Electrochemistry, 37, Kluwer Academic/Plenum Publisher, New York, 2004, pp. 131–251.
[6] A.L. Dicks, J. Power Sources 156 (2006) 128–141.
[7] M.A. Paisley, U.S. Patent 6,680,137 B2, Integrated Biomass Gasification and Fuel Cell System (2004).
[8] G. Donolo, G.D. Simon, M. Fermeglia, J. Power Sources 158 (2006) 1282–1289.
[9] C. Tomasi, M. Baratieri, B. Bosio, E. Arato, P. Baggio, J. Power Sources 157 (2) (2006) 765–774.
[10] K.D. Panopoulos, L.E. Fryda, J. Karl, S. Poulou, E. Kakaras, J. Power Sources 159 (1) (2006) 570–585.
[11] K.D. Panopoulos, L. Fryda, J. Karl, S. Poulou, E. Kakaras, J. Power Sources 159 (1) (2006) 586–594.
[12] H. Morita, F. Yoshiba, N. Woudstra, K. Hemmes, H. Spliethoff, J. Power Sources 138 (2004) 31–40.
[13] S.E. Chuck, Master Thesis, Illinois Institute of Technology, Chicago, 1966.
[14] R. Bajura, FutureGen Presentation, NETL, 2004.
[15] M. Onischak, D. Gidaspow, in: N.L. Norman (Ed.), Separation of Gaseous Mixtures by Regenerative Sorption on Porous Solids. Part II. Regenerative Separation Of CO_2, vol. II, Chemical Rubber Co., Cleveland, OH, 1972, pp. 71–93.
[16] D. Gidaspow, J. Jung, R.K. Singh, Powder Technol. 148 (2004) 123–141.
[17] V. Jiradilok, D. Gidaspow, J. Kalra, S. Damronglerd, S. Nitivattananon, Powder Technol. 164 (2006) 33–49.
[18] M. Driscoll, D. Gidaspow, Proceedings of the AIChE Annual Meeting, San Francisco, November 14, 2006.
[19] B.S. Baker, D. Gidaspow, D.T. Wasan, Thermal Phenomena in Fuel Cells and Batteries, vol. 8, Wiley/Interscience, New York, 1971, pp. 63–156.
[20] M. Farooque, G. Carlson, H.C. Maru, C. Bentley, Proceedings of the Third International Fuel Cell Conference, Nogoa, Japan, 1999, pp. 1–7.

[21] A. Weimer, Proceedings of the Seminar at IIT, University of Colorado Boulder, November 29, 2006.
[22] D. Gidaspow, B. Ettehadieh, Ind. Eng. Chem. Fundam. 22 (1983) 193–201.
[23] M. Syamlal, D. Gidaspow, AIChE J. 31 (1985) 127–135.
[24] D. Gidaspow, L. Huilin, in: L.S. Fan, T.M. Knowlton (Eds.), Fluidization, vol. IX, Engineering Foundation, 1998, pp. 661–668.
[25] N.A. Frankel, A. Acrivos, Chem. Eng. Sci. 22 (1967) 847–853.
[26] J. Jung, D. Gidaspow, J. Nanoparticle Res. 4 (2002) 197–483.
[27] H. Yoon, J. Wei, M.M. Denn, AIChE J. 24 (5) (1978) 885–903.
[28] F.D. Skinner, L.D. Smoot, in: L.D. Smoot, D.T. Pratt (Eds.), Heterogeneous Reaction of Char and Carbon, Plenum Press, New York, 1979, pp. 149–167.
[29] P.L. Walker Jr., F. Rusinko Jr., L.G. Austin, Adv. Catal. 2 (1959) 134.
[30] W.B. Cheng, C.Y. Wen, Computer Code for Moving Bed Coal Gasifier Simulation and Design, Submitted by C.Y. Wen to IGT for coal gasification data book, 1979.
[31] C.Y. Wen, Optimization of coal gasification processes, Research and development report no. 66, Interim report no.1, Contract no. 14-01-0001-497 with Office of Coal Research, U.S. Department of the Interior, Washington, DC, 1975.
[32] D.J. Dharia, Proceeding of the 12th Intersociety Energy Conversion Engineering Conference, vol. 1, Paper index no. 779056, 1977, pp. 337–340.
[33] D. Gidaspow, Final report: critical survey of mathematical modeling and experimental work in phosphoric acid and molten carbonate fuel cell, under contract no. DE AC02-76CH00016 with the United States Department of Energy, Brookhaven National Laboratory, Upton, New York, 1980.
[34] D. Gidaspow, in: H.C. Maru (Ed.), Proceeding of the Symposium on Porous Electrodes: Theory and Practice, vol. 84-8, The Electrochemical Society Inc., 1984, pp. 350–376.
[35] D. Gidaspow, Multiphase Flow and Fluidization: Continuum and Kinetic Theory Descriptions, 1st ed., Academic Press, 1994.
[36] J.A.M. Kuippers, B.P.B. Hoomans, W.P.M. van Swaaij, in: L.S. Fan, T.M. Knowlton (Eds.), Fluidization, vol. IX, Engineering Foundation, 1998, p. 15.
[37] R. Jackson, AlChE Symp. Ser. 301 (90) (1995) 1.
[38] H. Arastoopour, Powder Technol. 119 (2001) 59–67.
[39] G.D. Cody, D.J. Goldfarb, G.V. Storch Jr., A.N. Norris, Powder Technol. 87 (1996) 211–232.
[40] J. Jung, D. Gidaspow, I.K. Gamwo, Ind. Eng. Chem. Res. 44 (2005) 1329–1341.
[41] M. Tartan, D. Gidaspow, AIChE J. 50 (2004) 1760–1775.